COMPARATIVE STUDY OF THE STRUCTURE AND ELECTROSTRICTIVE PROPERTIES OF CHITOSAN-ZnO NANOPARTICLES AND CHITOSAN-Zn^{2+} ION NANO-BIOCOMPOSITE

Citlali Uitz Toalá[1], Evgen Prokhorov[2,a,*], Martin Adelaido Hernández-Landaverde[2], José Martin Yáñez Limón[2,b], José Juan Gervacio-Arciniega[3,c], Gabriel Luna-Barcenas[1,d]

[1] – Institute of Advanced Materials for Sustainable Manufacturing, Campos Queretaro, Av. Epigmenio González 500, Fraccionamiento San Pablo C.P. 76130, Santiago de Querétaro, Mexico

[2] – Centro de Investigación y de Estudios Avanzados del Instituto Politécnico Nacional, Unidad Querétaro, Libramiento Norponiente 2000. Fracc. Real de Juriquilla, C.P. 76230, Querétaro, México

[a] – ORCID: 0000-0003-1572-2420, [b] – ORCID: 0000-0001-6457-4044

[3] – La Benemérita, Universidad Autónoma de Puebla, SECIHTI-Facultad de Ciencias Físico Matemáticas, Avenida San Claudio y 18 Sur, Colonia San Manuel, C.P. 72570, Puebla México

[c] – ORCID: 0000-0001-7965-4493, [d] – ORCID: 0000-0002-1162-6928

**corresponding author: prokhorov@cinvestav.mx*

Abstract

This work aimed to investigate the electrostriction effect of two types of chitosan-zinc oxide films (CS-ZnO): non-neutralised - obtained by mixing CS and ZnO in acetic acid, and neutralised - films immersed in a NaOH solution. The X-ray, SEM, FTIR, AFM, weight, polarisation, and dielectric spectroscopy measurements indicate that these two films have different structures. In non-neutralised films, the chelation effect is observed due to the Zn^{2+} ions formed from ZnO under acidic conditions, causing an increase in the CS chain's dimension. In neutralised films, Zn^{2+} ions precipitate as nanoparticles (NPs). The difference in the structure is the reason for the difference in electrostrictive properties, a variation in the orientation of polymer chains in an electric field. Furthermore, the electrostriction coefficient M_{33} obtained for neutralised films with ZnO nanoparticles ($5.8 \cdot 10^{-1}$ m^2/V^2) is similar to or higher than that for poly(vinylidene fluoride)(PVDF)-based nanocomposites. CS-ZnO NP nanocomposite films are a promising option for biomedical applications.

Keywords: *chitosan, zinc oxide, chelation, electrostriction, interface layer*

Received: 23.02.2026
Accepted: 15.06.2026

1. Introduction

Electrostrictive polymers have attracted considerable attention recently due to their applications in sensors, energy harvesting, electronic devices, tissue engineering, and related fields. These polymers consist of flexible macromolecular chains whose alignment can be altered by applying an external electric field. As a result, polarisation occurs due to the rotation of polymer chains in the electric field, leading to electrostrictive strain and polymer deformation [1–3]. This effect occurs in all dielectric polymeric materials, but most publications report investigations of electrostriction in poly(vinylidene fluoride) (PVDF) and polyurethane (PU) [1–5]; however, electrostriction has also been observed in other polymers and nanocomposites [5–8]. Nonetheless, the fundamental electrostriction mechanism in polymers is still unclear [9–12]. Previous studies attributed the significant electrostrictive strain in PVDF-based polymers to their high dielectric constant, field-induced phase transition, charge displacement in the crystalline phase [9, 12, 13], and the orientation of the amorphous fraction that exists between the crystalline phases [9, 10–12].

For electrostrictive materials, strain S is given by the following phenomenological relation [9, 14, 15]:

$$S = Q \cdot \varepsilon_0 \cdot (\varepsilon_r - 1)^2 \cdot E^2 = M \cdot E^2 \quad (1)$$

where:

Q – charge-related electrostrictive coefficient [m^4/C^2];
ε_0 – permittivity of vacuum [F/m];
ε_r – material's dielectric constant;
E – applied electric field [V/m];
M – electrostrictive coefficient [m^2/V^2].

Therefore, it is necessary to increase the dielectric constant of polymers to improve their deformation and electrostriction properties. It has been reported that the dielectric constant of a PVDF-based material can be increased by mixing PVDF with fillers such as barium titanate ($BaTiO_3$) [14, 16, 17], reduced graphene oxide [17] and zinc oxide ZnO [18, 19]. It has been shown that the electrostriction coefficient tends to increase with increasing content of filler with a high dielectric constant [14, 16–19]. This explanation can be applied to PVDF-$BaTiO_3$ nanocomposites, in which the dielectric constant of PVDF is approximately 15 [20, 21] and that of $BaTiO_3$ nanoparticles is approximately 85–90 times higher than that of the polymer [14, 16]. However, this explanation cannot be applied directly in the case of PVDF-ZnO composites because the dielectric constant of ZnO is approximately 12–16 [22], which is comparable with that of PVDF. Therefore, another mechanism has been proposed to explain the increase in the electrostriction coefficient, based on the increasing of PVDF β phase [18, 20, 23].

These electrostrictive polymers may find biomedical applications in tissue engineering, biosensors, artificial muscles, actuators, and various medical instruments [4, 15]. For these applications, the development of biocompatible electrostrictive polymers is urgently needed. However, to the best of our knowledge, electrostriction effects for biopolymers have not been reported in the literature.

Chitosan (CS) is a natural biopolymer with high absorption capacity, biodegradability, biocompatibility, and antibacterial features. It is important to note that chitosan is a hydrophilic polymer with $–NH_2$/$–NH_3^+$ and –OH side groups that can interact with nanoparticles via hydrogen bonding, forming nanocomposites with new properties. Among various nanoparticles, zinc oxide nanoparticles (ZnO NPs) are the most frequently

studied for diverse applications (including biomedicine) due to their biocompatibility, biodegradability, and antibacterial properties [24]. It should be noted that there are numerous publications in the literature devoted to studying the properties of CS-ZnO NPs nanocomposites [25–33]; however, due to different methods for nanocomposite preparation, the articles need to be reviewed regarding results and explanations of electric, Fourier-transform infrared spectroscopy (FTIR), and X-ray diffraction (XRD) measurements. For example, some research reported the direct dissolution of ZnO NPs in a chitosan solution in acetic acid (a non-neutralised nanocomposite) [25–29]. It is, however, known that acetic acid reacts with ZnO NPs, resulting in the formation of Zn^{2+} ions [27]:

$$ZnO + 2\,HX \rightarrow Zn^{2+} + 2\,X^{-} + H_2O \quad (2)$$

Due to the presence of Zn^{2+} ions in the materials, a chelation effect is observed. Chelation is a reaction between a metal ion and an organic complexing agent, leading to the formation of a complex involving the amino and hydroxyl groups of CS and zinc ions, thereby affecting the structure of CS macromolecules [34–36].

In another method, a CS- and ZnO-containing solution or films containing Zn^{2+} ions were treated with a sodium hydroxide (NaOH) solution at 60–80 °C. In that case, the coordination bonds between Zn^{2+} and the –OH and $–NH_2$ groups of CS are disrupted; Zn^{2+} ions react with OH^- to form $Zn(OH)_2$, which is then converted to ZnO nanoparticles (neutralised films) [30–34].

Differences in CS-ZnO film preparation methods lead to variations in the structure and properties of the nanocomposites. Still, many studies have yet to address this difference. Despite the diversity of nanocomposite structures, materials prepared using both methods may be applied in sensors, energy harvesting, electronic devices, biomedicine, water purification, etc.

To the best of our knowledge, there is no information in the literature on the electrostrictive properties of the CS-Zn ions and CS-ZnO NPs materials. As mentioned above, the fundamental electrostriction mechanism in polymers is still unclear. [10–13]. It is expected that adding ZnO nanoparticles can increase the dielectric constant of the composites due to interfacial polarisation and increase the electrostrictive coefficient, as given by Equation 1. In addition, there are no reports on the electrostriction properties of polymers with the chelation effect. Therefore, this work aimed to study the structural properties of CS films with Zn^{2+} ions and CS-ZnO NPs, including their dielectric, polarisation, and electrostrictive properties and their dependence on the concentration of ZnO powder. The samples were characterised by SEM, FTIR, X-ray diffraction, impedance spectroscopy, polarisation measurements, and AFM analysis.

2. Materials and Methods

2.1. Materials

Chitosan (CS, high molecular weight, ~350 kDa, DD ≥ 76%) and ZnO NPs (~40 nm in diameter), dispersed in water, were purchased from Sigma-Aldrich (St. Louis, MO, USA). Acetic acid glacial mixture (99.7%) of analytical grade and 0.1 N NaOH analytical grade were purchased from J.T. Baker.

The 1 wt.% CS solution was prepared by dissolving CS in a 0.1 M aqueous acetic acid solution under sonication for 24 h at room temperature. ZnO sonicated colloidal solutions with various ZnO wt.% (3, 5, 8, 10, and 15 wt.% with regard to the CS) were dispersed in

the CS solution and stirred at 25000 rpm until the solution became homogeneous. The non-neutralised chitosan films were produced by pouring the chitosan solution into Petri dishes and drying for 24 h at 60 °C in an oven. Neutralised CS-ZnO NP films were obtained by immersing non-neutralised films in 0.1 N NaOH solution for 30 min at 60 °C, followed by washing with distilled water to remove Na^+ ions, then dried for 24 h at 60 °C in an oven. Film thickness ranged from 50 to 100 μm, as measured using a Mitutoyo micrometre with 1 μm resolution.

Films sputtered on both sides with gold created contacts for impedance and polarisation measurements.

2.2. Methods of Analysis

A scanning electron microscope (SEM (SEM-FE-JEOL JMS-7610), was used to observe the microstructure of the nanocomposites at 2 kV. Fourier-Transform Infrared Spectroscopy (FTIR) (Perkin Elmer spectrophotometer) was applied to examine the interaction between CS and the NPs within a 4000–800 cm^{-1} range. The crystalline structure of the films was determined by X-ray diffraction (XRD) using a Rigaku Dmax2100 diffractometer with Cu Kα radiation (λ = 1.5406 Å).

The moisture content, W [%], was calculated from the weight difference between the films annealed at various temperatures in the benchtop environmental chamber SU-261 for 30 min (W_0). An analytical balance of 0.0001 g accuracy was used. The dry sample's reference weight (W_d) was evaluated after drying at 170 °C. The following equation was used:

$$W = \frac{W_0 - W_d}{W_d} \cdot 100\% \quad (3)$$

Impedance measurements were carried out with an Agilent 4249 A, which has a frequency range of 40–100 MHz and a magnitude of 100 mV at room temperature. ZView software was used to calculate the resistance (R) and capacitance (C) at 100 Hz. This frequency was chosen to prevent the effects of contact and interface polarisation. The correlation between the conductivity (σ) and dielectric constant (ε) was determined using the following equation: $\sigma = d/(R \cdot S)$, $\varepsilon = C \cdot d/(\varepsilon_0 \cdot S)$, where d and S are the thickness and transversal area of the samples, respectively. All measurements were performed on 4 samples, which allowed to calculate the mean values and the standard deviation.

The measurements of polarisation (P-E loops) and strain dependence on the applied field (S-E loops) were obtained simultaneously in a measuring cell with parallel electrodes, immersed in silicone oil to avoid film breakdown. The P-E loop curve was measured by a Sawyer-Tower circuit with a Precision LC materials analyser (Radiant Technologies, Inc., with a TREK Model 609E-6 high-voltage amplifier). The strain was determined by utilising a photonic sensor and a fibre-optic interferometry system. S-E and P-E loops were measured simultaneously at 2 Hz. Measurements were performed using 10 triangular pulses with a period of 500 ms (or at 2 Hz). Consequently, the average value of 10 measurements was computed. The electrostriction coefficient M_{33} was calculated by fitting the strain-electric field dependence using a quadratic function. The M_{33} values for each film were subjected to Tukey's mean comparison tests at the 95% confidence level ($p < 0.05$).

The surface roughness was investigated using atomic force microscopy (AFM) using AFM-XE-7 Park Systems.

3. Results and Discussion

3.1. Structure Characterisation

XRD analysis can provide information about the crystalline structure of neutralised and non-neutralised films. The XRD pattern of the CS powder (Figure 1) shows the partially crystalline structure of chitosan, with two peaks at $2\theta \approx 9°$ and $2\theta \approx 21°$. This structure corresponds to the hydrate form of CS [37] and indicates chitosan's crystallinity due to intermolecular and extramolecular hydrogen bonding [38].

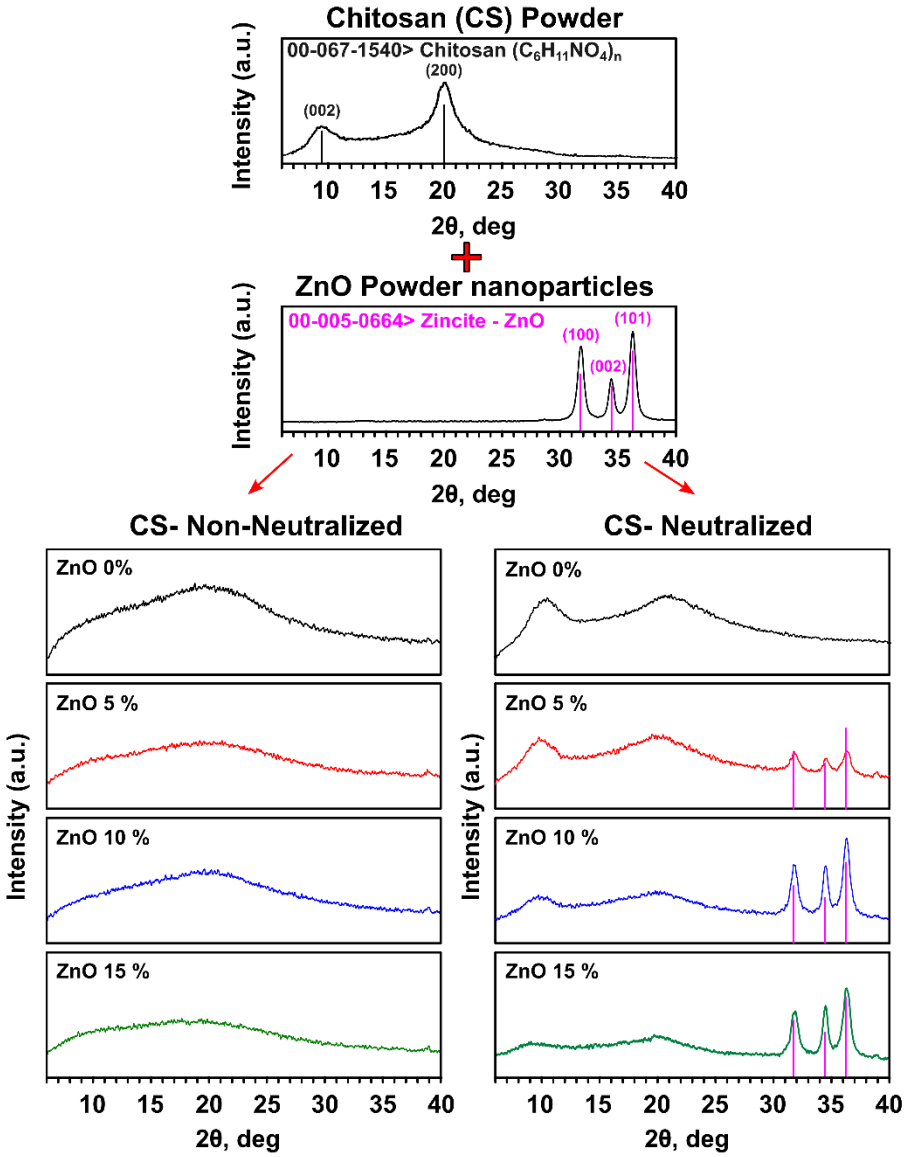

Figure 1. XRD pattern of CS powder, ZnO NPs, non-neutralised and neutralised films of different ZnO powder content (wt.%).

The CS films obtained from a solution of chitosan in acetic acid are almost amorphous due to residual solvent, as this environmental condition prevented the formation of inter- and intramolecular hydrogen bonds in CS and led to reduced packing [39]. The same amorphous structure of CS was observed for all the non-neutralised films with ZnO powders, as no CS diffraction peaks were observed. These measurements demonstrated that Zn ions were present in the non-neutralised films and that ZnO nanoparticles were absent.

In contrast, in pure CS-neutralised films, the same crystalline planes corresponding to the CS powder were observed due to the removal of acetate ions, indicating a more organised long-range structure and the restoration of inter- and intramolecular hydrogen bonds in CS (Figure 1) [40]. In addition, in the XRD patterns of the neutralised films with different wt.% ZnO powder, characteristic peaks at 2θ 31.7°, 34.4°, and 36.2° were detected (Figure 1), confirming the formation of ZnO NPs (JCPDS 00-036-1451) after neutralisation. The same results were presented in previous studies [30, 31].

The structural differences between neutralised and non-neutralised films can be further confirmed by SEM and AFM analyses. Figure 2 shows SEM images of ZnO NPs, CS-ZnO non-neutralised, and CS-ZnO neutralised films. The image of neat NPs shows that the particles are nearly spherical with a diameter of ~40 nm (Figure 2a). The surfaces of the non-neutralised films were smooth without any nanoparticles (Figure 2b). It should be noted that this type of surface is caused by Zn^{2+} chelation effect characteristic for CS-Zn^{2+} complex [34]. In contrast, the ZnO nanoparticles were clearly visible in the neutralised films. In the energy-dispersive X-ray spectroscopy (EDS) elemental maps of both non-neutralised and neutralised films, the main structural elements of chitosan (carbon, oxygen, and nitrogen) were identified in the presence of Zn (Figures 2c and 2e).

Figure 3 shows the surface topology of non-neutralised (Figure 3a) and neutralised (Figure 3b) films with 10 wt. % ZnO powder identified with AFM analysis. Differences in the morphology of the two films, similar to those observed in the SEM analysis, were found. As evidenced by the AFM images, the surface of the non-neutralised films was smooth, with a root-mean-square roughness (Sq) of 3.7 nm, and contained no nanoparticles. However, in neutralised films, the surface roughness increases significantly, reaching an Sq of 8.3 nm, due to ZnO NPs embedded in the polymer matrix.

The XRD, SEM, and AFM measurements confirm the difference in the structures of the neutralised and non-neutralised films, and the results suggest that the ZnO in the non-neutralised films is transformed into Zn^{2+} ions according to reaction Equation 2 due to interactions with acetic acid. In contrast, ZnO NPs with a crystalline structure in NaOH-treated films appear due to the neutralisation. A similar conclusion can be made from photographs of CS-Zn^{2+} and CS-ZnO NP films (Figure 4). Films containing Zn^{2+} ions are transparent, suggesting formation of a homogeneous, molecular-level complex, while chitosan films containing ZnO nanoparticles are opaque due to light scattering by the suspended solid particles.

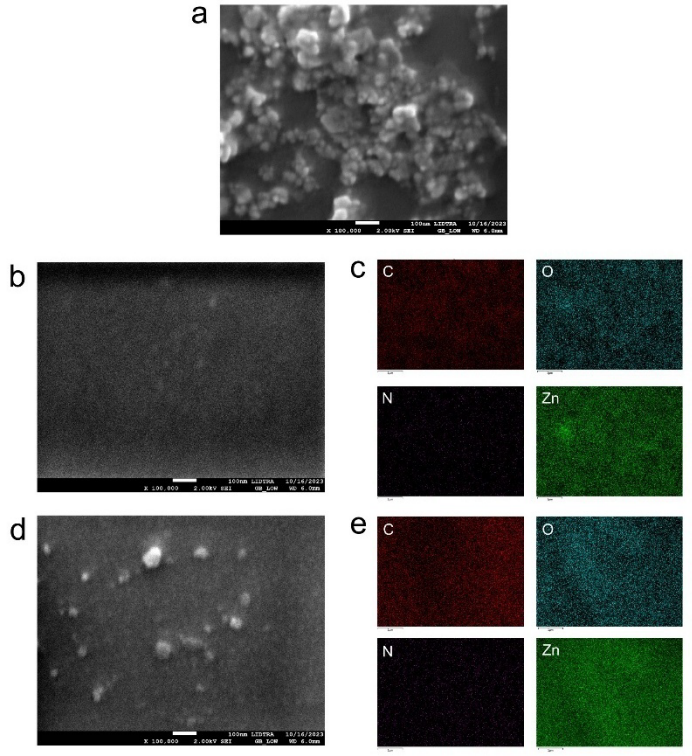

Figure 2. SEM micrograph of (a) neat ZnO NPs, (b) non-neutralised and (d) neutralised films with 10 wt.% of ZnO powder, and EDS compositional elemental mapping of (c) non-neutralised and (e) neutralised films.

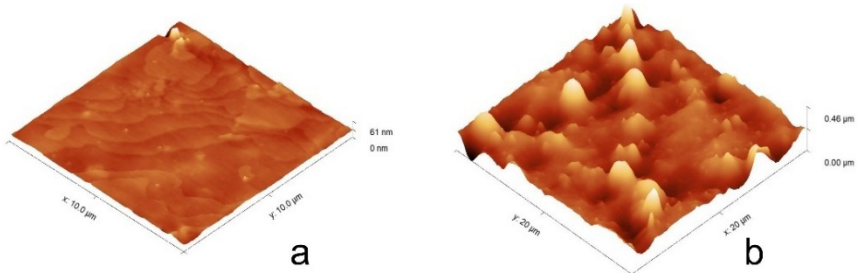

Figure 3. AFM images of (a) non-neutralised and (b) neutralised films of 10 wt.% ZnO.

(a) **(b)**

Figure 4. Photograph of (a) non-neutralised and (b) neutralised films.

FTIR spectra were recorded to confirm the interactions between CS and Zn^{2+} ions through the chelation mechanism in non-neutralised materials and the most possible interaction mechanism in neutralised CS films with ZnO NPs. Figure 5a shows typical FTIR absorbance spectra of neat non-neutralised and neutralised CS films, CS-Zn^{2+} ions, and CS-ZnO NP materials.

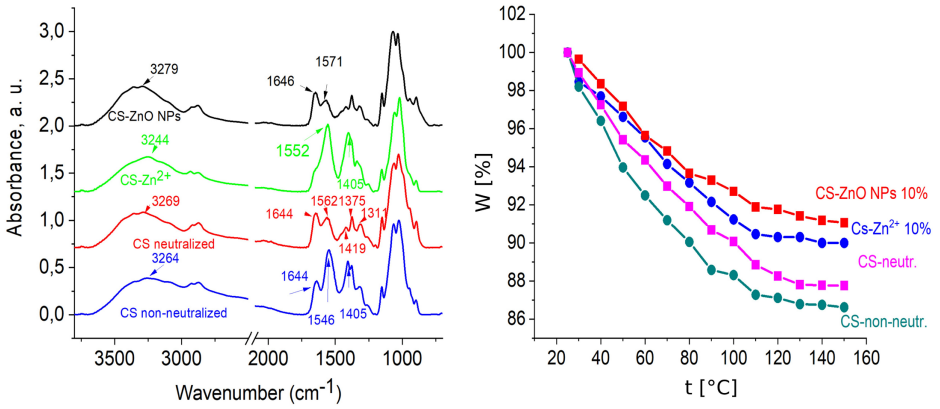

(a) **(b)**

Figure 5. (a) FTIR spectra of CS-Zn^{2+} and CS-ZnO NPs films, (b) dependency of the moisture content on the annealing temperature in the non-neutralised and neutralised films.

The neat non-neutralised and neutralised CS film spectra exhibited characteristic bands between 3700 and 3000 cm^{-1}, corresponding to the overlap of the stretching vibrations of -OH and -NH groups and the amide I band at 1644 cm^{-1}. On the other hand, the spectrum of the non-neutralised chitosan film has two strong bands at 1546 and 1405 cm^{-1} due to the presence of carboxylate ions and protonation of the amine group of chitosan. In the FTIR spectra of the neutralised films, these peaks are replaced by the N-H bending peak at 1562 cm^{-1}. The removal of acetate ions was further confirmed by the disappearance of a band at 1419 cm^{-1} and the appearance of peaks at 1419, 1375, and 1311 cm^{-1}, corresponding to CH_2 bending, CH_3 deformation, and CH_2 wagging, respectively. These changes in the spectrum allowed us to conclude that the films were neutralised entirely and that the acetic acid ions were removed [41, 42].

Some noticeable differences were observed in the spectra of the non-neutralised CS-ZnO films compared to those of the non-neutralised CS. The wide band corresponding to the overlap of the stretching vibrations of -OH and -NH groups centred at 3264 cm^{-1} shifts to 3244 cm^{-1}, the intensity of the band at 1644 cm^{-1} decreases, and the band at 1546 cm^{-1} related to the carboxylate ion and the protonated amine group of chitosan shifts to 1552 cm^{-1}. All these changes indicated the formation of coordination bonds and the chelation process between the -NH and -OH groups of CS and Zn^{2+} ions, which changed the structure of the non-neutralised films [36, 43, 44].

The change in the FTIR spectra of the neutralised CS-ZnO NPs films was less drastic. Compared to pure neutralised CS films, the characteristic peaks of -OH and -NH- groups were shifted to a higher wavenumber of 3279 cm^{-1}. A similar phenomenon was observed for the band attributed to vibrations in the $-NH_2$ group, which shifted to 1571 cm^{-1} due to the formation of hydrogen bonds between the ZnO NPs and CS [30, 45]. The differences

in the structures of the non-neutralised and neutralised ZnO films cause differences in the dielectric and electrostrictive properties, as described in the following sections.

Another confirmation of the interaction between the CS side groups and the Zn^{2+} ions in non-neutralised and ZnO NPs in neutralised films can be obtained by measuring the dependence of the water content in the films. Weight loss is observed in all films at temperatures ranging from 20 to 150 °C due to the evaporation of bound water from the CS in the amorphous region [46]. Therefore, the weight loss in the non-neutralised films was higher than in neutralised ones (Figure 5b). In addition, as the concentrations of Zn^{2+} ions and ZnO NPs increase, the water content decreases. FTIR measurements show that the amino and hydroxyl groups of CS bond to Zn^{2+} ions and ZnO NPs; therefore, as the ZnO powder concentration increases, the water content decreases.

3.2. Impedance and Electrostriction

Figure 6 shows the dependence of the conductivity and dielectric constant of the non-neutralised and neutralised films as a function of the wt.% of ZnO powder. The conductivity (σ) of both films decreases with increasing ZnO powder content (Figure 6a). The conductivity of neat CS is related to the Grotthuss mechanism, in which protons move along hydrated molecules within the hydrogen-bonding network via a hopping process [46]. As a result of the interaction of reactive CS side groups with Zn^{2+} ions in non-neutralised films and with nanoparticles in neutralised films (based on FTIR measurements), both the number of generated protons and the number of hydrated molecules decrease. This effect is a reason for the decrease in the film's conductivity.

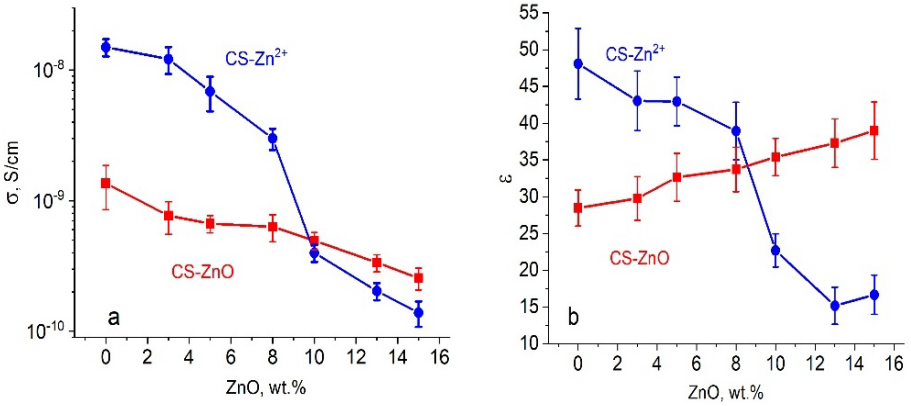

Figure 6. The dependences of (a) conductivity and (b) dielectric constant of the non-neutralised and neutralised films as a function of ZnO content.

The dielectric constant (ε) for the CS-Zn^{2+} ions decreases with increasing ZnO content (Figure 6b). The dielectric constant of dry (water content < 1%) non-neutralised chitosan films equals approximately 6 [37]. The high value of ε in the as-prepared films is associated with high water content, indicating the formation of a CS chain-bonded water complex that contributes to the dielectric properties [46]. Consequently, a decrease in water content with increased Zn^{2+} ions reduces the dielectric constant.

In contrast, in CS-ZnO NPs neutralised films, the dielectric constant increases with increasing ZnO content (Figure 6b). Considering that the dielectric constant (ε) of ZnO NPs is approximately 12–15 (decrease with increasing particle size [22]) and that the ε of

as-prepared neat, neutralised CS films is approximately 27. Therefore, all the models of a mixture of two materials must demonstrate a monotonic decrease in the effective dielectric constant with increasing concentration of ZnO NPs in CS [47]. Recent studies have explained the increase in ε in polymer-dielectric NP composites by assuming the formation of an "interface" region at the interfaces between the polymer and dielectric nanoparticles [48, 49]. This layer can also be formed in CS-ZnO NPs neutralised films due to the hydrogen bonding between ZnO and CS, as observed in FTIR spectra. Such interfacial interactions between CS and ZnO NPs can increase the dielectric constant and the interfacial charge, affecting the electrostrictive properties of nanocomposites.

Figures 7a and 7c present the polarisation-field (P-E) and the corresponding strain-electric field (S-E) loops (Figures 7b and 7d) measured at room temperature in neat CS films (non-neutralised and neutralised), as well as films of CS-Zn^{2+} and CS-ZnO NPs with 5, 10, and 15 wt.% of ZnO powder. The measured P-E loops in neat CS films fail to saturate and remain open due to leakage current, likely caused by absorbed water in the CS matrix [50]. In contrast, a linear relationship between the polarisation and electric field was observed for the CS-Zn^{2+} and CS-ZnO films, indicating that these materials are linear dielectrics [10].

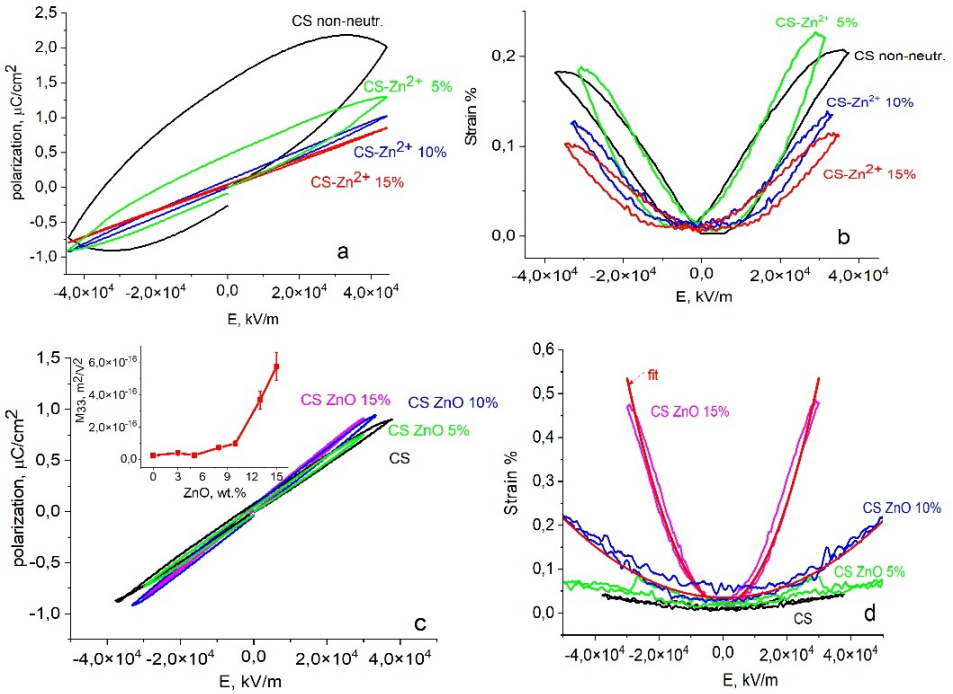

Figure 7. The polarisation-field (P-E) ((a) and (c)) and the corresponding strain-electrical field (S-E) loops ((b) and (d)) measured at room temperature in neat non-neutralised and neutralised CS films of 0, 5, 10, and 15 ZnO wt.%. The inset in Figure 7c shows the dependence of M33 on the concentration of NPs measured in CS-ZnO NP films.

The S-E curves of the CS-Zn^{2+} films have a shape that is close to parabolic but has hysteresis, which indicates a deviation from the typical electrostrictive effect. Furthermore, the deformation decreases as Zn ion concentration increases (Figure 7b).

Such a hysteresis region on the S-E curves was observed in materials based on PVDF and was associated with field phase transition, field conformational transformation of chains [51], charge displacement in the crystalline phase [7, 13], an oriented amorphous fraction, the existence of crystalline and amorphous fractions [10–12], or properties of the relaxor system [6]. These explanations cannot be directly applied to CS-ZnO films. To the best of our knowledge, there are no reports in the literature on the electrostrictive effect of chelated polymer-ionic materials or the effect of ion concentration on electrostrictive deformation. In contrast, in the CS-ZnO NPs films, the strain obeys a quadratic function of the electric field (Figure 7d). Fitting by a parabolic function (Equation 1) allows obtaining M_{33}, the electrostrictive coefficient, and its dependence on the concentration of ZnO NPs. With increasing concentration of ZnO NPs, M_{33} increases, as shown in the inset of Figure 7c.

The fundamental electrostriction mechanism in polymers remains unclear [10–13]. Table 1 summarises the various explanations for the high electrostrictive effects of PVDF-based polymers, the most-studied electrostrictive materials. Additionally, the table contains the values of the dielectric constant and electrostriction coefficient. The most common explanation for the high electrostriction effect in PVDF-based polymers is associated with phase transformation and an increase in the β-phase. However, according to the XRD data, no phase transformations are observed in the CS-ZnO NPs films; nevertheless, the electrostriction coefficient is higher than that of many PVDF-based materials.

Based on the results obtained, the electrostrictive properties of the CS-Zn^{2+} ions and CS-ZnO NPs films can be explained as follows. Figure 8 shows the proposed mechanism of the electrostriction effect. Non-neutralised CS contains protonated -NH_3^+ groups, acetate ions, and water molecules. Therefore, in an external electric field, the orientation of CS-NH_3^+ with the positive charge is responsible for a higher electrostriction effect than that of neutralised CS with neutral -NH_2 groups (Figure 8b).

In the case of CS-Zn^{2+}, due to the chelation effect, interactions between zinc ions and the amino and hydroxyl groups of CS are observed (FTIR spectroscopy). In the former mechanism, Zn^{2+} ions bind to these functional groups on several adjacent CS chains, acting as bridges between the chains and forming a larger-dimensional supramolecular complex (Figure 8c) [36, 52].

According to the literature, the electrostriction response depends on the chain length [53, 54]. As the concentration of Zn^{2+} increases, the number of long chains increases, reducing their ability to rotate and decreasing the electrostriction strain. This effect is probably responsible for the hysteresis observed in the S-E dependence. In addition, reducing the water content (Figure 5b) decreases the dielectric constant (Figure 6b). These two effects led to a decrease in strain value as the concentration of Zn^{2+} increased.

In the case of the neutralised CS-ZnO NPs films, despite the decrease in the amount of water, the dielectric constant of the materials increased (Figure 6) due to the formation of an interfacial layer surrounding the ZnO NPs (Figure 8). The interface layer increases the dielectric constant and interface charge [18, 19]. The electrostriction coefficient increases with increasing concentration of ZnO NPs (Figure 7c, inset). In addition, in the hexagonal crystal structure of ZnO NPs, Zn^{+2} ions can move inside the cell and contribute to the electrostriction coefficient (Figure 8c) [55].

Table 1. The values of dielectric constant (ε), electrostrictive coefficient M_{33}, and electrostriction mechanism reported in PVDF-based materials.

Material	ε	M_{33} [m^2/V^2]	Mechanism	Ref
P(VDF-TrFE-CFE)-$BaTiO_3$ 1 wt.%	37.1	$4.42 \cdot 10^{-18}$	change of phase composition and increasing of ε	[15]
P(VDF-TrFE-CFE)	32.8	$1.31 \cdot 10^{-18}$	-	
P(VDF-TrFE-CFE)-$BaTiO_3$ 2 wt.%	43.5	-	increasing of dielectric constant	[18]
P(VDF-TrFE-CFE)-TiO_2 10 wt.%	43	-	increasing of dielectric constant	
PVDF-HFP/Co-ZnO 2 wt.%	35	-	increasing of β-phase	[20]
P(VDF-HFP)	5.8	$3.7 \cdot 10^{-16}$	-	[21]
P(VDF-HFP)/ZnO 20 wt.%	11.6	$8.9 \cdot 10^{-16}$	increasing of β-phase and dielectric constant	
P(VDF-HFP)/ZnO nanorods	38	-	increasing of β-phase and filler orientation	[56]
P(VDF-TrFE-CTFE)	29.5	$1.3 \cdot 10^{-18}$	electrically induce phase transition and preferred orientation of dipoles	[9]
P(VDF-TrFE-CTFE)	-	-	conformation transformation of oriented polymer chains in the amorphous phase	[57]
P(VDF–TrFE) proton irradiation	9	$1.76 \cdot 10^{-18}$	a transformation between the nonpolar and polar phases induced by an electric field	[58]
P(VDF–TrFE) electron irradiation	10	$2.2 \cdot 10^{-18}$	phase transformation between the ferroelectric β and the paraelectric α phase	[16]
PVDF	-	$1.7 \cdot 10^{-17}$	space charge migration to traps	[59]
CS-ZnO NPs 15 wt.%	39	$5.8 \cdot 10^{-16}$		This work

Note. TrFE - trifluoroethylene; CFE - chlorofluoroethylene; HFP - poly(vinylidene fluoride-*co*-hexafluoropropylene); CTFE - chlorotrifluoroethylene.

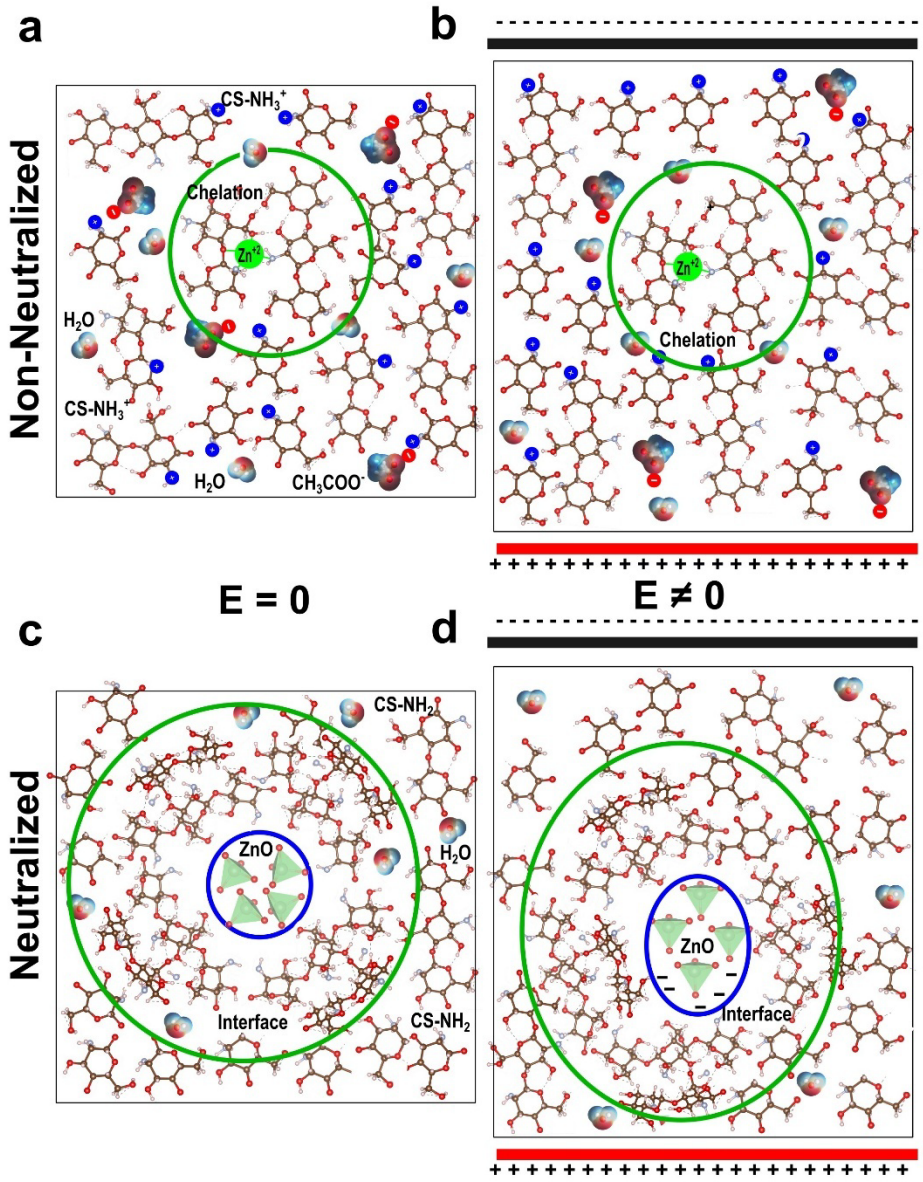

Figure 8. A schematic image of the proposed mechanism of the electrostriction effect in (a, b) non-neutralised and (c, d) neutralised films.

4. Conclusions

This work reports the electrostrictive properties of chitosan-ZnO films. Depending on the preparation method, two different film structures were obtained. This difference is not considered in many publications on CS-ZnO materials, leading to contradictory experimental results. In the case of non-neutralised films, due to the conversion of ZnO to Zn^{2+} ions and the chelation effect, the electrostriction strain decreases as the Zn ion concentration increases. Zn^{2+} ions may be bound by the side groups of CS chains, which

leads to an increase in the length of the chains and a decrease in their ability to rotate in an external electric field.

On the other hand, in neutralised films, the transformation of Zn^{2+} ions into crystalline ZnO NPs occurs. In this case, due to hydrogen-bond interactions between the ZnO NPs and the surrounding CS matrix, an interface layer with a high dielectric constant and additional interface polarisation is observed. Therefore, as the concentration of NPs increases, the electrostriction coefficient also increases. The proposed mechanism for the electrostriction effect differs significantly from the electrostriction mechanism described in the literature for PVDF-based nanocomposites. Moreover, the study results show the possibility of obtaining a new electrostrictive biopolymer with an electrostriction coefficient comparable to or higher than that of PVDF-based nanocomposites. These CS-ZnO NPs nanocomposite films are promising candidates for biomedical applications.

5. Acknowledgements

The authors are grateful to J.A. Muñoz Salas for technical assistance in dielectric measurements, R.A. Mauricio-Sánchez for FTIR measurements, E. Urbina Alvarez for SEM measurements, and R. Flores Farias for P-E measurements.

6. Author Contributions

Conceptualisation, E.P.; formal analysis, M.A.H.-L.; investigation, C.U.T., E.P., M.A.H.-L., J.M.Y.L., and J.J.G.-A.; writing—original draft preparation, C.U.T.; writing—review and editing, E.P. and G.L.-B. All authors have read and agreed to the published version of the manuscript.

7. References

[1] Yao S, Yuan J; (2022) Electrostrictive polymer nanocomposites: fundamental and applications. In: Nanocomposites: Preparation, Characterization and Modeling, John Wiley & Sons, Ltd, pp. 213–239. **DOI:** 10.1002/9781394150427.ch8

[2] Carpi F (ed.); (2016) Electromechanically Active Polymers: A Concise Reference. Springer International Publishing, Cham. **DOI:** 10.1007/978-3-319-31530-0

[3] Diguet G, Cavaille J-Y, Sebald G, Takagi T, Yabu H, Suzuki A, Miura R; (2021) Physical behaviour of electrostrictive polymers. Part 1: Polarization forces. Computational Materials Science 190, 110294. **DOI:** 10.1016/j.commatsci.2021.110294

[4] Kochervinskii VV, Gradov OV, Gradova MA; (2022) Fluorine-containing ferroelectric polymers: applications in engineering and biomedicine. Russian Chemical Reviews 91(11), RCR5037. **DOI:** 10.57634/RCR5037

[5] Maksimkin AV, Dayyoub T, Telyshev DV, Gerasimenko AYu; (2022) Electroactive polymer-based composites for artificial muscle-like actuators: a review. Nanomaterials 12(13), 2272. **DOI:** 10.3390/nano12132272

[6] Cottinet P-J, Guyomar D, Guiffard B, Lebrun L, Putson C; (2010) Electrostrictive polymers as high-performance electroactive polymers for energy harvesting. In: Suaste-Gomez E (ed.), Piezoelectric Ceramics, Sciyo, pp. 185–208. **DOI:** 10.5772/9946

[7] Ning C, Zhou Z, Tan G, Zhu Y, Mao C; (2018) Electroactive polymers for tissue regeneration: Developments and perspectives. Progress in Polymer Science 81, 144–162. **DOI:** 10.1016/j.progpolymsci.2018.01.001

[8] Jaffri SB, Ahmad KS; (2022) Systematic investigation of the revolutionary role of electroactive polymers in modifying microelectromechanical systems. In: Inamuddin, Ahamed MI, Boddula R, Gabouri AA (eds.), Electroactive Polymeric Materials, 1st ed., CRC Press, Boca Raton, pp. 101–118. **DOI:** 10.1201/9781003173502

[9] Lheritier P, Vaxelaire N, Tencé-Girault S, Domingues Dos Santos F, Defay E; (2020) Influence of field-induced phase transition on poly(vinylidene fluoride-trifluoroethylene-chlorotrifluoroethylene) strain. Physical Review Applied 14(4), 044061. **DOI:** 10.1103/PhysRevApplied.14.044061

[10] Ignat M, Ovezea D, Hamciuc E, Hamciuc C, Dimitrov L; (2014) Study on the electromechanical properties of polyimide composites containing TiO2 nanotubes and carbon nanotubes. Journal of Polymer Research 21(8), 536. **DOI:** 10.1007/s10965-014-0536-y

[11] Rui G, Huang Y, Chen X, Li R, Wang D, Miyoshi T, Zhu L; (2021) Giant spontaneous polarization for enhanced ferroelectric properties of biaxially oriented poly(vinylidene fluoride) by mobile oriented amorphous fractions. Journal of Materials Chemistry C 9(3), 894–907. **DOI:** 10.1039/D0TC04632A

[12] Huang Y *et al.*; (2021) Enhanced piezoelectricity from highly polarizable oriented amorphous fractions in biaxially oriented poly(vinylidene fluoride) with pure β crystals. Nature Communications 12(1), 675. **DOI:** 10.1038/s41467-020-20662-7

[13] Zhu Z, Rui G, Li R, He H, Zhu L; (2021) Enhancing electrostrictive actuation via strong electrostatic repulsion among field-induced nanodomains in a relaxor ferroelectric poly(vinylidene fluoride- *co* -trifluoroethylene- *co* -chlorotrifluoroethylene) random terpolymer. ACS Applied Materials & Interfaces 13(35), 42063–42073. **DOI:** 10.1021/acsami.1c12745

[14] Li F, Jin L, Xu Z, Zhang S; (2014) Electrostrictive effect in ferroelectrics: An alternative approach to improve piezoelectricity. Applied Physics Reviews 1(1), 011103. **DOI:** 10.1063/1.4861260

[15] Pawlik B, Schirrmann C, Bornhorst K, Costache F; (04/09/2013) Strain-enhanced nanoparticle electrostrictive polymer blends for actuator applications. In Proceedings of SPIE, San Diego, California, USA. **DOI:** 10.1117/12.2011715

[16] Zhang S, Huang C, Klein RJ, Xia F, Zhang QM, Cheng Z-Y; (2007) High performance electroactive polymers and nano-composites for artificial muscles. Journal of Intelligent Material Systems and Structures 18(2), 133–145. **DOI:** 10.1177/1045389X06063341

[17] Kulkarni ND, Kumari P; (2023) Role of rGO on mechanical, thermal, and piezoelectric behaviour of PVDF-BTO nanocomposites for energy harvesting applications. Journal of Polymer Research 30(2), 79. **DOI:** 10.1007/s10965-023-03449-4

[18] Pawlik B, Schirrmann C, Bornhorst K, Costache F; (2014) Strain-enhanced nanocomposites of electrostrictive polymers and high-k nanofillers for micro-actuation applications. Procedia Engineering 87, 1601–1604. **DOI:** 10.1016/j.proeng.2014.11.531

[19] Erol İ, Khamidov G, Acar F; (2025) Bioengineered ZnO-enhanced CS-based nanocomposites: synergistic tuning of dielectric, electrical, and surface properties

for next-gen flexible electronics. Journal of Polymer Research 32(8), 273. **DOI:** 10.1007/s10965-025-04487-w

[20] Parangusan H, Ponnamma D, Al-Maadeed MAA; (2018) Stretchable electrospun PVDF-HFP/co-ZnO nanofibers as piezoelectric nanogenerators. Scientific Reports 8(1), 754. **DOI:** 10.1038/s41598-017-19082-3

[21] Tohluebaji N, Thainiramit P, Putson C, Muensit N; (2021) Phase and structure behavior vs. Electromechanical performance of electrostrictive P(VDF-HFP)/ZnO composite nanofibers. Polymers 13(15), 2565. **DOI:** 10.3390/polym13152565

[22] Anandhavelu S, Dhanasekaran V, Sethuraman V, Park HJ; (2017) Chitin and chitosan based hybrid nanocomposites for super capacitor applications. Journal of Nanoscience and Nanotechnology 17(2), 1321–1328. **DOI:** 10.1166/jnn.2017.12721

[23] Yadav D, Tyagi N, Yadav H, James A, Sareen N, Kapoor M, Kumar K, Kataria Y, Singhal K; (2023) Effect of various morphologies and dopants on piezoelectric and detection properties of ZnO at the nanoscale: a review. Journal of Materials Science 58(26), 10576–10599. **DOI:** 10.1007/s10853-023-08680-4

[24] Asture A, Rawat V, Srivastava C, Vaya D; (2023) Investigation of properties and applications of ZnO polymer nanocomposites. Polymer Bulletin 80(4), 3507–3545. **DOI:** 10.1007/s00289-022-04243-w

[25] Aadnan I, Zegaoui O, Daou I, Esteves Da Silva JCG; (2020) Synthesis and physicochemical characterization of a ZnO-Chitosan hybrid-biocomposite used as an environmentally friendly photocatalyst under UV-A and visible light irradiations. Journal of Environmental Chemical Engineering 8(5), 104260. **DOI:** 10.1016/j.jece.2020.104260

[26] Praveen E, Murugan S, Jayakumar K; (2015) Nano ZnO embedded in chitosan matrix for vibration sensor application. In AIP Conference Proceeding, Rome, Italy. **DOI:** 10.1063/1.4917673

[27] Saisa, Agusnar H, Alfian Z, Nainggolan I; (2020) Polymer of chitosan with ZnO addition to optimize high responsivity and sensitivity in sensor film. In AIP Conference Proceeding, Penang, Malaysia. **DOI:** 10.1063/5.0016439

[28] Türemen M, Demir A, Gokce Y; (2021) The synthesis and application of chitosan coated ZnO nanorods for multifunctional cotton fabrics. Materials Chemistry and Physics 268, 124736. **DOI:** 10.1016/j.matchemphys.2021.124736

[29] Boura-Theodoridou O, Giannakas A, Katapodis P, Stamatis H, Ladavos A, Barkoula N-M; (2020) Performance of ZnO/chitosan nanocomposite films for antimicrobial packaging applications as a function of NaOH treatment and glycerol/PVOH blending. Food Packaging and Shelf Life 23, 100456. **DOI:** 10.1016/j.fpsl.2019.100456

[30] Azimi N, Gandomkar A, Sharif M; (2023) Relationship between production condition, microstructure and final properties of chitosan/graphene oxide–zinc oxide bionanocomposite. Polymer Bulletin 80(6), 6455–6469. **DOI:** 10.1007/s00289-022-04277-0

[31] Li L-H, Deng J-C, Deng H-R, Liu Z-L, Xin L; (2010) Synthesis and characterization of chitosan/ZnO nanoparticle composite membranes. Carbohydrate Research 345(8), 994–998. **DOI:** 10.1016/j.carres.2010.03.019

[32] Shaba EY, Jacob JO, Tijani JO, Suleiman MAT; (2021) A critical review of synthesis parameters affecting the properties of zinc oxide nanoparticle and its application in wastewater treatment. Applied Water Science 11(2), 48. **DOI:** 10.1007/s13201-021-01370-z

[33] Girigoswami K, Viswanathan M, Murugesan R, Girigoswami A; (2015) Studies on polymer-coated zinc oxide nanoparticles: UV-blocking efficacy and in vivo toxicity. Materials Science and Engineering: C 56, 501–510. **DOI:** 10.1016/j.msec.2015.07.017

[34] Meulenkamp EA; (1998) Size dependence of the dissolution of ZnO nanoparticles. The Journal of Physical Chemistry B 102(40), 7764–7769. **DOI:** 10.1021/jp982305u

[35] Alshraiedeh NH, Ammar OF, Masadeh MM, Alzoubi KH, Al-Fandi MG, Oweis RJ, Alsharedeh RH, Alabed RA, Hayajneh RH; (2022) Comparative study of antibacterial activity of different ZnO nanoparticles, nanoflowers, and nanoflakes. Current Nanoscience 18(6), 758–765. **DOI:** 10.2174/1573413718666220303153123

[36] Han J, Qiu W, Gao W; (2010) Potential dissolution and photo-dissolution of ZnO thin films. Journal of Hazardous Materials 178(1–3), 115–122. **DOI:** 10.1016/j.jhazmat.2010.01.050

[37] Kyzas GZ, Siafaka PI, Pavlidou EG, Chrissafis KJ, Bikiaris DN; (2015) Synthesis and adsorption application of succinyl-grafted chitosan for the simultaneous removal of zinc and cationic dye from binary hazardous mixtures. Chemical Engineering Journal 259, 438–448. **DOI:** 10.1016/j.cej.2014.08.019

[38] Mutlu N, Liverani L, Kurtuldu F, Galusek D, Boccaccini AR; (2022) Zinc improves antibacterial, anti-inflammatory and cell motility activity of chitosan for wound healing applications. International Journal of Biological Macromolecules 213, 845–857. **DOI:** 10.1016/j.ijbiomac.2022.05.199

[39] Salama HE, Abdel Aziz MS; (2020) Novel biocompatible and antimicrobial supramolecular O-carboxymethyl chitosan biguanidine/zinc physical hydrogels. International Journal of Biological Macromolecules 163, 649–656. **DOI:** 10.1016/j.ijbiomac.2020.07.029

[40] Spoială A *et al.*; (2022) The development of antimicrobial chitosan ZnO nanocomposite membranes for water purification. Romanian Journal of Materials 52(1), 17–25.

[41] Kumar-Krishnan S, Prokhorov E, Ramírez M, Hernandez-Landaverde MA, Zarate-Triviño DG, Kovalenko Y, Sanchez IC, Méndez-Nonell J, Luna-Bárcenas G; (2014) Novel gigahertz frequency dielectric relaxations in chitosan films. Soft Matter 10(43), 8673–8684. **DOI:** 10.1039/C4SM01804D

[42] Ma G, Qian B, Yang J, Hu C, Nie J; (2010) Synthesis and properties of photosensitive chitosan derivatives. International Journal of Biological Macromolecules 46(5), 558–561. **DOI:** 10.1016/j.ijbiomac.2010.02.009

[43] Wang SF, Shen L, Tong YJ, Chen L, Phang IY, Lim PQ, Liu TX; (2005) Biopolymer chitosan/montmorillonite nanocomposites: Preparation and characterization. Polymer Degradation and Stability 90(1), 123–131. **DOI:** 10.1016/j.polymdegradstab.2005.03.001

[44] Gartner C, López BL, Sierra L, Graf R, Spiess HW, Gaborieau M; (2011) Interplay between structure and dynamics in chitosan films investigated with solid-state NMR, dynamic mechanical analysis, and X-ray diffraction. Biomacromolecules 12(4), 1380–1386. **DOI:** 10.1021/bm200193u

[45] Mekahlia S, Douadi T; (2022) Chitosan–ZnO nanocomposite from a circular economy perspective: in situ cotton-used fabric recycling and the nanocomposite recovering. Polymer Bulletin 79(9), 7491–7529. **DOI:** 10.1007/s00289-021-03859-8

[46] Noriega SE, Subramanian A; (2011) Consequences of neutralization on the proliferation and cytoskeletal organization of chondrocytes on chitosan-based matrices. International Journal of Carbohydrate Chemistry 2011, 1–13. **DOI:** 10.1155/2011/809743

[47] Guan B, Ni W, Wu Z, Lai Y; (2009) Removal of Mn(II) and Zn(II) ions from flue gas desulfurization wastewater with water-soluble chitosan. Separation and Purification Technology 65(3), 269–274. **DOI:** 10.1016/j.seppur.2008.10.037

[48] Huang C, Liao H, Liu X, Xiao M, Liao S, Gong S, Yang F, Shu X, Zhou X; (2022) Preparation and characterization of vanillin-chitosan Schiff base zinc complex for a novel Zn2+ sustained released system. International Journal of Biological Macromolecules 194, 611–618. **DOI:** 10.1016/j.ijbiomac.2021.11.104

[49] Qiu B, Xu X, Deng R, Xia G, Shang X, Zhou P; (2019) Construction of chitosan/ZnO nanocomposite film by in situ precipitation. International Journal of Biological Macromolecules 122, 82–87. **DOI:** 10.1016/j.ijbiomac.2018.10.084

[50] González-Campos JB, Prokhorov E, Luna-Bárcenas G, Sanchez IC, Lara-Romero J, Mendoza-Duarte ME, Villaseñor F, Guevara-Olvera L; (2010) Chitosan/silver nanoparticles composite: Molecular relaxations investigation by dynamic mechanical analysis and impedance spectroscopy. Journal of Polymer Science Part B: Polymer Physics 48(7), 739–748. **DOI:** 10.1002/polb.21941

[51] Ioelovich M; (2014) Crystallinity and hydrophility of chitin and chitosan. Journal of Chemistry 3(3), 7–14.

[52] Barber P, Balasubramanian S, Anguchamy Y, Gong S, Wibowo A, Gao H, Ploehn HJ, Zur Loye H-C; (2009) Polymer composite and nanocomposite dielectric materials for pulse power energy storage. Materials 2(4), 1697–1733. **DOI:** 10.3390/ma2041697

[53] Zhang Q-P, Du F-Y, Liu X, Lv J-H, He L, Li J-L, Li Y-T, Zhou Y-L; (2023) Optimizing the dielectric constant of the shell layer in core–shell structures for enhanced energy density of polymer nanocomposites. Physical Chemistry Chemical Physics 25(27), 18030–18037. **DOI:** 10.1039/D3CP01367G

[54] Saeed A, Guizani I, Hanash FE, Asnag GM, Al-Harthi AM, Alwafi R, Qahtan TF, Morsi MA, Assran AS; (2024) Enhancing optical, structural, thermal, electrical properties, and antibacterial activity in chitosan/polyvinyl alcohol blend with ZnO nanorods: polymer nanocomposites for optoelectronics and food/medical packaging applications. Polymer Bulletin 81(13), 11645–11670. **DOI:** 10.1007/s00289-024-05270-5

[55] Toalá CU, Prokhorov E, Barcenas GL, Landaverde MAH, Limón JMY, Gervacio-Arciniega JJ, De Fuentes OA, Tapia AMG; (2023) Electrostrictive and piezoelectrical properties of chitosan-poly(3-hydroxybutyrate) blend films. International Journal of Biological Macromolecules 250, 126251. **DOI:** 10.1016/j.ijbiomac.2023.126251

[56] Wang Y, Xu M, Zhang F, Wang Y, Zhang L, Zhang Q, Deng Y; (2021) Design on orientation of one-dimensional ZnO/P(VDF-HFP) nanocomposites for significant enhanced electromechanical conversion. Composites Science and Technology 204, 108635. **DOI:** 10.1016/j.compscitech.2020.108635

[57] Wongwirat T, Zhu Z, Rui G, Li R, Laoratanakul P, He H, Manuspiya H, Zhu L; (2020) Origins of electrostriction in poly(vinylidene fluoride)-based ferroelectric polymers. Macromolecules 53(24), 10942–10954. **DOI:** 10.1021/acs.macromol.0c02083

[58] Lam TY, Lau ST, Chan HLW, Choy CL, Cheung WY, Wong SP; (2005) Modification of the structure and properties of poly(vinylidene fluoride–trifluoroethylene) 56/44 mol % copolymer by a proton-irradiation treatment. Journal of Polymer Science Part B: Polymer Physics 43(17), 2334–2339. **DOI:** 10.1002/polb.20524

[59] Hughes OR; (2007) Frequency dependence of hysteresis associated with the electromechanical performance of PVDF film. Journal of Polymer Science Part B: Polymer Physics 45(23), 3207–3214. **DOI:** 10.1002/polb.21102

© Polish Chitin Society

Open Access: This article is distributed under the terms of the Creative Commons Attribution 4.0 International License (CC BY 4.0), which permits use, sharing, adaptation, distribution and reproduction in any medium or format, provided that appropriate credit is given to the original author(s) and source, a link to the license is provided, and any changes are indicated. Third-party material is included under the same license unless otherwise stated in a credit line.